Stochastic Environmental Research and Risk Assessment manuscript No.
(will be inserted by the editor)

Stochastic Modeling of Solar Irradiance during Hurricanes

Luis Ceferino · Ning Lin · Dazhi Xi

Received: date / Accepted: date

Abstract The unprecedented growth of solar generation adoption indicates that solar can become a significant source of modern and clean energy for our power grids in just a few decades. Despite solar's growing criticality for generation, few studies have proposed models to assess solar generation during natural disasters. In particular, hurricanes bring environmental conditions that may drastically reduce solar generation even if solar infrastructure remains fully functional. Here, we present a stochastic model to quantify irradiance decay during hurricanes. The model is developed through mixed-effect regression on a dataset that merges historical Global Horizontal Irradiance and Atlantic hurricane activity, exhibiting higher irradiance decays for higher hurricane categories and closer to the hurricane center. Accordingly, our model describes the irradiance decay as a function of hurricane category and the distance the hurricane center normalized by the hurricane size. We show that category-dependent shapes and scales increase the statistical performance of the irradiance decay function based on the Akaike Information Criterion. Similarly, the hurricane's radius of outermost closed isobar performs best as normalizing distance. Our study suggests that hurricanes reduce irradiance due to optically thick clouds that absorb and reflect light. These clouds are close to the hurricane center and often become thicker during intensification. To showcase the methodology's applicability, we use it to generate stochastic simulations

L. Ceferino
The Andlinger Center for Energy and the Environment, Princeton University
Civil and Urban Engineering Department, New York University
370 Jay St, Brooklyn, NY 11201
Tel.: +1-646-997-0534
E-mail: ceferino@nyu.edu

N. Lin
Civil and Environmental Engineering Department, Princeton University
D. Xi
Civil and Environmental Engineering Department, Princeton University

of irradiance in the Southern United States during a synthetic storm from its genesis to its dissipation. Our results also show that generation in Miami-Dade, Florida, can decrease beyond 70% in large regions during a category-4 synthetic hurricane even if the solar infrastructure is undamaged. Furthermore, generation losses can also last beyond three days, and this timeframe will be exacerbated if solar panels become non-functional. Our follow-up study integrates our proposed model with panel fragility functions to offer analysis capabilities for forecasting time-varying solar generation during hurricanes.

Keywords Disaster resilience · Solar panels · Solar irradiance · Hurricanes · Optically thick clouds

1 Introduction

Solar generation is becoming a pillar in modern power systems. Solar energy accounted for nearly 40% of all the new electric generating capacity installed on the U.S. grid in 2019, the highest share in its history (Perea et al., 2019). The rapid adoption of panels to harvest solar energy is transforming key power system features such as its economics, environmental contributions to global warming, and resilience (Moriarty and Honnery, 2016). These new power system features may be a crucial part of our future grids, and government projections state that solar generation will be 20–30% of the global electricity by 2050 (International Energy Agency, 2014; Shah and Booream-Phelps, 2015; The International Renewable Energy Agency, 2018; Solaun and Cerdá, 2019). Research has already highlighted and projected solar energy's long-term environmental (Solangi et al., 2011; Creutzig et al., 2017) and economic (Devabhaktuni et al., 2013; Kannan and Vakeesan, 2016) benefits. However, there is significantly less understanding of the benefits of solar generation for increasing the resilience of our vulnerable existing grids.

Hurricanes have exposed significant vulnerabilities in our power grids. For example, Hurricane Maria caused the total loss of power in multiple major cities in Puerto Rico in 2017, leaving regions without power for up to eight months (Wang et al., 2018; Campbell et al., 2018). Similarly, in mainland United States, Hurricane Sandy in 2012 left more than eight million customers without power across 21 states (Henry and Ramirez-Marquez, 2016). Solar generation can increase resilience through decentralization, a fundamental paradigm switch where users can generate energy locally, e.g., through rooftop solar panels (Colson et al., 2011; Panteli and Mancarella, 2015; Wang et al., 2016). Only a recent investigation has proposed a framework based on risk analysis to quantify the resilience of modern power systems with rooftop solar panels, but exclusively for earthquake hazards (Patel et al., 2021; Ceferino et al., 2020). As hurricanes pose an enormous threat to urban centers worldwide, this paper focuses on building a cornerstone solar irradiance model that enables the risk analysis of modern power systems with solar generation during hurricanes (generally called tropical cyclones).

Unlike earthquakes, hurricanes bring environmental conditions that may drastically reduce solar generation even if solar infrastructure remains fully functional. Figure 1 exemplifies the effect of hurricanes on the spatial distribution of solar irradiance and thus generation. The plot shows Global Horizontal Irradiance (GHI) at 3pm UCT (9 am local time) when Hurricane Katrina made landfall in Louisiana as a category three event in 2005 compared to the GHI distribution the year after. The comparison shows that the hurricane reduced GHI even for sites that were hundreds of kilometers away from the hurricane center. This observation is consistent with recent findings on GHI decay during past hurricanes (Cole et al., 2020). Yet, to integrate this observation into a risk analysis framework that assesses solar generation resilience, we lack a predictive model that generalizes GHI reduction under hurricanes, i.e., parametrizing GHI decay with key hurricane features.

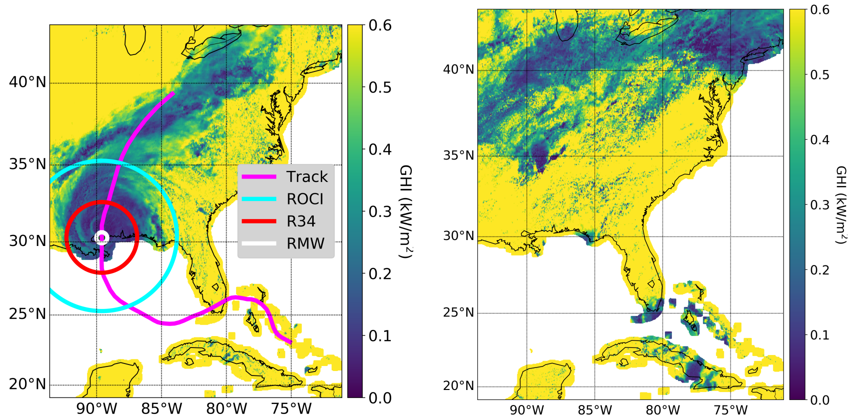

(a) 2005 (during hurricane Katrina)

(b) 2006 (one year after hurricane Katrina)

Fig. 1: Global horizontal irradiance decay during hurricanes with two snapshots at the same time but in different years. Both plots show the spatial distribution of GHI on August 29th, at 3 pm UTC (or 10 am local time in Lousiana). (a) The plot shows GHI in 2005 during Hurricane Katrina, indicating the hurricane's track, radius of maximum wind, radius at a wind speed of 34 knots, and radius of the outermost closed isobar. (b) The plot shows GHI in 2006 in the same region at the same time. Data retrieved from NREL (Sengupta et al., 2018).

To fill this research gap, we conduct an extensive data analysis on historical GHI during the hurricane seasons from 2001 to 2017 by combining the hurricane Best Track Database (Landsea and Franklin, 2013) with a GHI database from the National Renewable Energy Laboratory (NREL) (Sengupta et al., 2018). The analysis identifies hurricane features that best predict the intensity and extent of GHI decay. Next, we develop a probabilistic mixed-effects model to capture irradiance decay through different functional forms. These functions describe time and space-varying GHI reduction factors from the hurricane center to unaffected regions using critical hurricane features with different model complexities. We fit the different functional forms and highlight the best predictive model based on the Akaike Information Criterion (AIC).

In application, we propose to first estimate solar irradiance when and where a hurricane occurs but for normal conditions (Sengupta et al., 2018). Then, we adjust the GHI estimates to the hurricane condition using our proposed probabilistic model for hurricane-induced GHI decay. Because the proposed GHI decay model is built for different times of the day and throughout the entire hurricane season, our integrative framework quantifies the time-series of solar irradiance for any real or synthetically simulated tropical cyclone since its landfall to dissipation.

To showcase our proposed methodology's broad and regional applicability for irradiance modeling, we use the framework to simulate solar generation for a synthetic storm in the United States's southern region. We compare our modeling results to existing studies on GHI decay to analyze its performance. This application demonstrates that this methodology can successfully simulate spatiotemporal distributions of irradiance under varying hurricane conditions from genesis to dissipation. Ceferino et al. (2021) integrates the proposed model with fragility functions for panel failure due to high winds to assess time-varying solar generation during hurricanes in residential or utility-scale panel arrays. These integrative approaches demonstrate the importance of GHI decay models for assessing the resilience of power systems with solar infrastructure to hurricanes.

The rest of the article begins with a statistical analysis of GHI during historical storms. Then, it proposes a probabilistic model for capturing GHI decays during hurricanes. Next, it shows the application to the Southern United States. Finally, the article provides a summary and conclusions of our analysis.

2 Analysis of GHI during historical storms

Hurricane conditions reduce solar irradiance intensity at the ground level over large geographical extents, limiting the ability of PV panels to harvest energy in communities. Figure 1 shows intense GHI decays during Hurricane Katrina in most regions within the radius (R34) at a wind speed of 17 ms^{-1} (34 knots), which reached 262 km. In some regions, intense decays extended to distances similar to the radii of the outermost closed isobar (ROCI), which reached 556 km. While Figure 1 shows only a snapshot for one hurricane demonstrating irradiance decays, we consistently observe the same trend in other hurricanes. In contrast to cloudless conditions of clear skies, which are associated with maximum solar generation, hurricanes cover extensive regions with different cloud structures from the eyewall to the rainbands (Houze, 2010). These clouds absorb and scatter light, reducing direct incident radiation and generally leading to lower GHI and reduced solar panel generation (Xie et al., 2016, 2019). Clouds that have high moisture density and vertical depth, i.e. optically thick clouds, can drastically reduce direct incident radiation (Nouri et al., 2019). Accordingly, hurricanes can significantly and rapidly lessen generation through optically thick cloud structures such as large cumulonimbus. However, hurricanes can also reduce generation significantly even with less optically thick cloud structures like stratiform clouds because they can cover large geographical extents.

To systematically investigate the effect of hurricanes on irradiance, we coupled a large dataset of GHI with historical hurricane data. We used the Physical Solar Model (PSM) version 3 from the National Solar Radiation Database (NSRDB) published by the National Renewable Energy Laboratory (NREL) to extract GHI with high spatial and temporal resolution (Sengupta et al., 2018). The PSM combines satellite-derived atmospheric and land surface properties with radiative transfer models to solve solar radiation through the Earth's atmosphere. The PSM provides solar irradiance at a 4-km horizontal resolution for 30-minute intervals from 1998 to 2017. The PSM enable us to observe the GHI behavior at different timesnaps for different hurricanes since 1998 for multiple sites and under various hurricane conditions.

2.1 Historical hurricane dataset

We compiled hurricane data from the revised Atlantic hurricane database (HURDAT2) (Landsea and Franklin, 2013). The data contain multiple hurricane features and span several decades; however, key spatial information including hurricanes' radii is only available since 1998. The hurricane data include ROCI, the radius of maximum wind (RMW), radius at wind speeds of 17 ms^{-1} (R34, 34 knots) and 33 ms^{-1} (R64, 64 knots), hurricane category, and maximum wind speeds. The hurricane data have a 3-hour temporal resolution, which is coarser than the PSM temporal resolution; thus, we reduced the granularity of the GHI dataset from 30 minutes to 3 hours and matched the hurricane recording times. After performing a preliminary assessment to estimate the geographical extent impacted by the hurricane, we collected GHI records from the 4$\times$4-km spatial grid within two times ROCI from the hurricane center, which reached several hundreds of kilometers for massive storms.

We analyzed 22 hurricanes whose geneses were in the North American basin, made landfall on the Atlantic coasts of Central and North America and the Caribbean, and whose lifetime maximum intensity reached a category of at least three. The intensity threshold filtered out the disproportionately large number of storms that did not reach high intensities. While these events' maximum intensities were high, we tracked them from landfall to dissipation, covering the full range of intensities from high categories until they weakened into tropical depressions. 22 events had tropical storm winds in their lifespan, and nine reached a category of 5 (Figure S1).

The 22 hurricanes cover an extensive geographical region of our assessment (Figure 2). These hurricanes have a wide variety of conditions, with maximum wind speeds up to 80 ms^{-1} (category 5), ROCI from 200 km to above 800 km, RMW up to 250 km, and radii at circulating wind speeds of 0 (R0) from 200 km to above 2000 km (Figure S1). HURDAT2 omitted R0, the shortest distance where hurricane circulating wind effects dissipate entirely. [1] Thus, we estimated R0 with a wind profile model that captures the radial structure of tropical cyclones (Chavas et al., 2015).

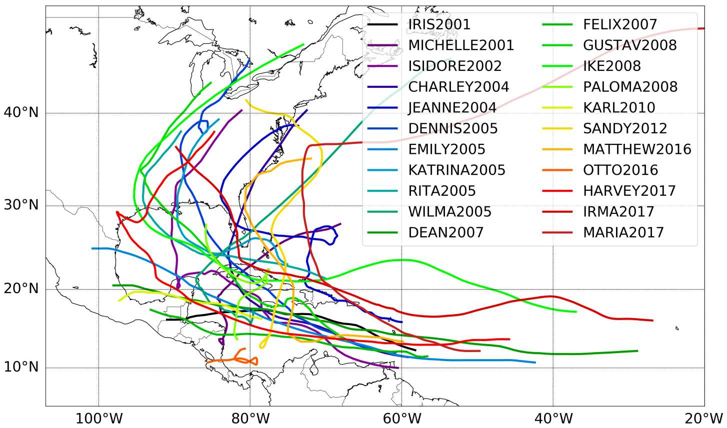

Fig. 2: List of hurricanes and their tracks included in GHI decay assessment in the North American basin

2.2 Key features for predicting GHI during hurricanes

To characterize GHI decay under different hurricane conditions, we define I^h as GHI during a hurricane. Previous research shows that GHI has strong temporal and spatial variability during normal conditions, i.e., no hurricane (Lehr et al., 2017; Patel et al., 2018). We account for such variability and characterize GHI deviations from normal conditions in the logarithm space as

$$\delta^h = ln\left(\frac{I^h}{\bar{I}}\right) \tag{1}$$

where $\bar{I}$ represents the median of the GHI under normal conditions at the same location and at the same time of the year as I^h. Since multiplicative factors capture clouds' effects on solar irradiance, i.e., Beer-Bouguer-Lambert law of extinction (Liou, 2002; Xie et al., 2019), we assume δ^h, in the logarithmic

[1] Notice that there is environmental wind at R0.

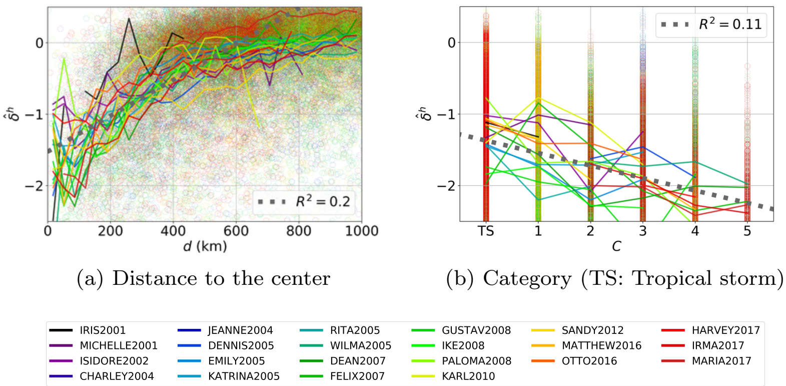

(a) Distance to the center

(b) Category (TS: Tropical storm)

Fig. 3: Scatter plots showing relationship between GHI decay and key hurricane features. $\widehat{\delta^h}$ during different hurricanes have different color. For each hurricane, the plots show a running average for $\widehat{\delta^h}$ using solid lines. The plots also show linear regressions in dotted lines and their corresponding R^2 values when the multi-hurricane data is lumped together. For visual clarity, there are only 50k randomly sampled data points in each plot.

space, can capture hurricane effects on GHI. We used 20 years of GHI data to estimate $\overline{I_{t,j}}$ for all the geographical extent covered by the hurricanes using a 3-hour temporal resolution. We used 20 years of GHI data to estimate $\bar{I}$ for all the geographical extent covered by the hurricanes using a 3-hour temporal resolution. We assume that at each time of the day, GHI has approximately the same distribution for a given month. As a result, we used approximately 600 instead of 20 data points to estimate the GHI medians. For example, to estimate GHI at 10 a.m. in June, we lumped the data of its days from 1998 to 2017. We observe that for sites farther from the center of the hurricane, the median of δ^h approaches zero, implying that the site is outside the area where hurricanes reduce GHI, i.e., $\bar{I} = \overline{I^h}$.

We analyzed GHI during the 22 hurricanes to estimate the samples $\widehat{\delta^h}$ and understand GHI behavior during different hurricane conditions. Because our focus was only on times of the day when communities can generate energy, we only included in our analysis daytime data where and when $\bar{I} > 10$ W-h/m^2, which finally resulted in ~28M data points. Figure 3 shows $\widehat{\delta^h}$ as a function of distance from the site to the hurricane's center and category.

Figure 3a shows the relationship between distances to the hurricane center d and $\widehat{\delta^h}$. On average, $\widehat{\delta^h}$ has reduced values for small d and grows steadily up to a plateau close to 0 for d values larger than 600 km. We fitted a line with d below 600 km to account mainly for the sites with significant irradiance decays and found an R^2 of 0.2 (correlation $\rho = 0.45$). We observe that the fitted line is not able to represent the transition between small distances to the plateau for large d where hurricanes have little effect. The observed transition is consistent with the spatial distribution of cloud optical thicknesses in hurricanes. Hurricane eyewalls, which surround the hurricane eye typically at 10-50 km from the center (Weatherford and Gray, 1988), are composed of optically thick clouds as a result of high moisture densities and large vertical depths (Kokhanovsky and von Hoyningen-Huene, 2004; John et al., 2020), thus significantly reducing direct incident radiation through high absorption and reflection. Outside the eyewall, clouds' optical thicknesses are high only in rainbands and significantly lower in between them. Outside the regions with rainbands, a regular combination of clear-sky and partially cloudy conditions arise, bringing GHI back to normal levels (Kokhanovsky and von Hoyningen-Huene, 2004; Luo et al., 2008; John et al., 2020). Figure 3a shows that this occurs beyond 600 km from the hurricane center.

Additionally, we find that high hurricane intensity exacerbates GHI decay. To focus on sites with the largest hurricane decay and cover areas within hurricane eyewalls, we analyzed sites located at 100km or less from the hurricane center. Figure 3b shows a decaying trend between hurricane category C and $\widehat{\delta^h}$ values, indicating that more intense hurricanes induce larger reductions in solar irradiance. A similar trend is observed between $\widehat{\delta^h}$ and maximum winds V (Figure S2a) because V has high colinearity with C as the latter variable is an increasing step function of V. Thus, we see that the linear fit performs very similarly with R^2 of nearly 0.11 (ρ = -0.34) in both cases. Lower irradiance levels for higher hurricane categories are also consistent with recent evidence on satellite-derived cloud microphysical features during hurricanes (John et al., 2020). There are larger regions with higher cloud optical thicknesses associated with large and thick cloud structures such as cumulonimbus during hurricane maturity and intensification rather than during hurricane development or dissipation.

To investigate hurricane size effect, we evaluated the relationship between different hurricane size metrics and both the intensity and geographical extent of GHI decay. To study whether GHI decays are larger for bigger hurricanes, we analyzed the relationship between $\widehat{\delta^h}$ and ROCI, RMW, and R0, respectively. We observe that hurricane size does not intensify GHI decay as linear fits between the size metrics and $\widehat{\delta^h}$ have low R^2 values of 0, 0.05, and 0.02, respectively (Figure S2).

To study how hurricane size correlates with the geographical extent of GHI decay, we analyzed the relationship between GHI and distance to the storm's center normalized by the hurricane size. We normalized d by four hurricane size metrics, ROCI, RMW, R0, and R34, where R34 is the radius at which the maximum wind speed is 34 knots, the minimum speed for the event to be categorized as a tropical storm. We split the data by hurricane category because C showed predictive power for hurricane decay intensification (Figure 3).

When the distance is normalized by ROCI and R34, we generally observe better fitting performance than for the absolute distance, with improved performance for higher hurricane categories (Figure 4 and S5). We estimated that a linear fit between $R = d/\text{ROCI}$ and $\widehat{\delta}^h$ has an R^2 of 0.38 for category 5, almost twice the value found for absolute distance for all storms (Figure 3a). For $R = d/\text{R34}$, R^2 values show comparably good fitting performance to using ROCI as normalizing distance (Table S1). The slopes of linear fits are steeper for higher categories, further demonstrating that the intensity of the hurricane intensifies GHI decay. As discussed earlier, this feature of GHI decay is driven by optically thicker cloud structures occurring during hurricane maturity and intensification. Distances normalized by RMW and R0 give lower performance, which, however, still illustrate how the effect of the hurricane on irradiance dissipates for large enough values of d (Figure S3 and S4).

The analysis also shows that the regions with GHI decay easily extend beyond RMW and R34 as they only define hurricanes' inner-core circulation (Table S1). In contrast, the regions with significant GHI decay do not reach R0 but are close to being bounded by ROCI. Thus, these observation suggests that the outer structure and radial extent of circulation bounded by ROCI is coupled with the cloud structures absorbing and reflecting light during hurricanes.

3 Developing GHI decay model through mixed-effects regression

To leverage well-established mixed-effects regression models (Pinheiro and Bates, 2006), we assume that $ln(I^h)$ is Gaussian, i.e., I^h is lognormaly distributed, during daytime, when generation is not negligible, i.e., $I^h > 0$. Thus

$$ln(I^h) = ln\big(\overline{I^h}\big) + \epsilon^h \tag{2}$$

where $\overline{I^h}$ is the GHI median, and ϵ^h is a Gaussian random variable with zero mean that accounts for the variability of GHI during hurricanes in the logarithmic space. We also assume that hurricanes reduce median GHI from normal conditions to $\overline{I^h}$ such that in the logarithmic space

$$ln(I^h) = ln(\bar{I}) + f(R, C) + \epsilon^h \tag{3}$$

where $\bar{I}$ is the median GHI during normal conditions, and $f(R, C)$ is a reduction factor that is function of the normalized distance to the hurricane's center R and the hurricane category C. f uses both R and C because they demonstrated to have good predictive power for GHI decay in the previous section. Using the expression in Equation 1, then

$$\delta^h = f(R, C) + \epsilon^h \tag{4}$$

Using Equation 4 and the samples of δ^h from our dataset, we conducted a mixed-effect regression analysis to test multiple functional forms $f(R, C)$ and formulate a predictive model for irradiance decay during hurricanes.

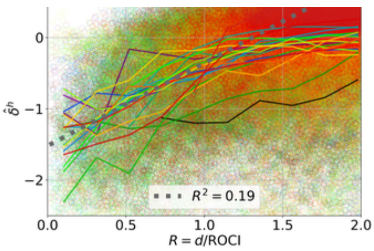

(a) Tropical storm

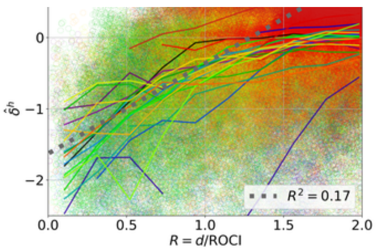

(b) Category 1

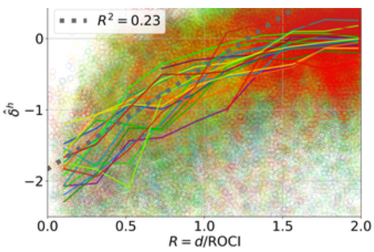

(c) Category 2

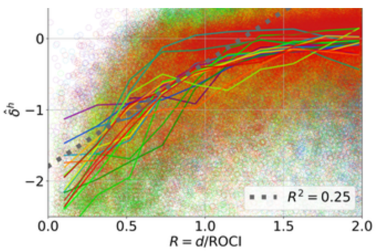

(d) Category 3

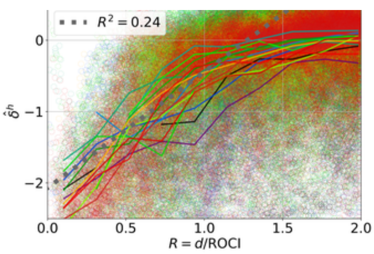

(e) Category 4

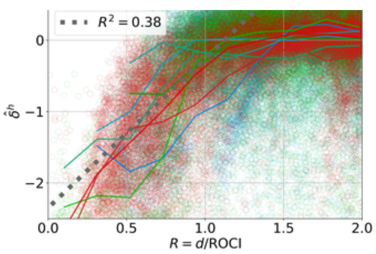

(f) Category 5

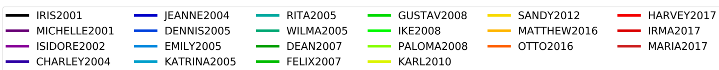

Fig. 4: Scatter plot showing relationship between GHI decay and distance normalized by ROCI for multiple categories. For each hurricane, the plots show a running mean for $\widehat{\delta^h}$ using solid lines. Linear trends are fitted for R between 0 and 1.2 when the multi-hurricane data is lumped together. There are 10k randomly sampled data points in each plot.

3.1 Functional forms for GHI reduction factors

We tested four different functional forms for $f(R, C)$. These functions are shown in Equation 5. All of them include a logarithmic growth as a function of R followed by a plateau when $f(R, C)$ reaches 0. The functional forms include a short-distance correction factor b and a scale factor c that further calibrate the influence of R on the irradiance decay. The short-distance correction factor is added to the value of R so that the logarithmic function approaches the observed values rather than $-\infty$ when the site is close to the center of the hurricane, i.e., $R \to 0$. The scale factor further normalizes R to define where the plateau is reached.

While all of the functional forms include a slope that varies with the hurricane category $(a_1C + a_2)$, they vary in their complexity, differing in the representation of the short-distance correction factor b and the scale factor c. In the functional form f_1 in Equation 5a, b and c remain constant for all hurricane categories. In the functional form f_2 in Equation 5b, b varies with category but c remains constant, and in the functional form f_3 in Equation 5c, b is constant and c varies with hurricane category. In the functional form f_4 in Equation 5d, both b and c vary with hurricane category.

$$f_1(R,C) = \begin{cases} (a_2C + a_1) \times ln\left(\frac{R+b}{c}\right) & \text{if } R + b < c \\ 0 & \text{if } R + b \geq c \end{cases} \tag{5a}$$

$$f_2(R,C) = \begin{cases} (a_2C + a_1) \times ln\left(\frac{R+(b_2C+b_1)}{c}\right) & \text{if } R + (b_2C + b_1) < c \\ 0 & \text{if } R + (b_2C + b_1) \geq c \end{cases} \tag{5b}$$

$$f_3(R,C) = \begin{cases} (a_2C + a_1) \times ln\left(\frac{R+b}{c_2C+c_1}\right) & \text{if } R + b < c_2C + c_1 \\ 0 & \text{if } R + b \geq c_2C + c_1 \end{cases} \tag{5c}$$

$$f_4(R,C) = \begin{cases} (a_2C + a_1) \times ln\left(\frac{R+(b_2C+b_1)}{c_2C+c_1}\right) & \text{if } R + (b_2C + b_1) < c_2C + c_1 \\ 0 & \text{if } R + (b_2C + b_1) \geq c_2C + c_1 \end{cases} \tag{5d}$$

3.2 Mixed-effects model formulation for GHI decay

We used a mixed-effects model to capture the main observed features of irradiance decay during hurricanes. Unlike other methods such as fixed-effects model, this model allows us to explicitly decompose the random variable ϵ^h in Equation 4 into two independent factors (Pinheiro and Bates, 2006), one factor accounting for the variability between different time steps represented by the random variable η^h and another accounting for the spatial variability at a fixed time represented by the random variable ε^h.

$$\delta^h = f(R,C) + \eta^h + \varepsilon^h \tag{6}$$

Through this explicit decomposition, we properly represent the high GHI temporal and spatial variability structrure as extensively discussed in previous research (Lehr et al., 2017; Patel et al., 2018; Mihailović et al., 2021). The mixed-effects regression has both fixed and random components (Pinheiro and Bates, 2006). With the fixed effect component, we capture how hurricanes decrease the (logarithm of the) median GHI with the factor $f(R,C)$ (Equation 5). With the random component of the model, we capture spatial uncertainty at a time step with a within-time random effect ε^h and uncertainty across time steps with a between-time step random effect η^h. The model assumes that η^h and ε^h are independent. Similar techniques and independence assumptions have been used to model natural disaster intensities with radiating decay. For example, mixed-effects models and similar independence assumptions are extensively used to assess ground shaking that propagates from an earthquake epicenter to a large geographical extent (Campbell and Bozorgnia, 2014; Abrahamson et al., 2016).

3.3 Fitting the GHI decay model

We lumped all hurricane data to fit the parameters of $f(R, C)$. Notice that for a fixed time t, an observation of δ^h at site j ($\delta^h_{t,j}$) is the sum of η^h_t, $\varepsilon^h_{t,j}$ and $f(R_{t,j}, C_t)$. As η^h_t only captures temporal uncertainty, at a fixed time t, it takes the same value for all sites. $\varepsilon^h_{t,j}$ captures spatial uncertainty, thus at fixed time t, it varies for each specific site j. Similarly, while C_t varies at each time step t, $R_{t,j}$ also varies for each site j. Thus, for each observation,

$$\delta^h_{t,j} = f(R_{t,j}, C_t) + \eta^h_t + \varepsilon^h_{t,j} \tag{7}$$

As described previously, we estimated $\delta^h_{t,j}$ for around ∼28 M observations corresponding to multiple time steps and sites of GHI recordings during the 22 hurricanes in the NREL dataset. We preprocessed the data by removing sites at long distances where hurricanes did not have significant effect on GHI, i.e., d/ROCI>2, d/RMW>20, d/R0>1, and d/R34>4 (Table S1). We then balanced the observations across the hurricane categories and distances from the center to the sites. There are more data samples for smaller hurricane categories and at larger distances from the center. To avoid that these samples heavily control the regression, we randomly selected the same number of samples for different categories and four equally spaced intervals of R, resulting in ~ 0.75 M data points for the analysis.

We conducted mixed-effect regressions for all 16 combinations of functional forms $f(R, C)$ and normalizing radii. We estimated the model parameters using maximum likelihood estimation (MLE) for the non-linear mixed-effects regression with a Matlab package. The package uses an expectation-maximization algorithm to solve for the parameters of the fixed component in Equation 5 while accounting for the unobserved component of the regression in Equation 7 (Lindstrom and Bates, 1990). We fitted the parameters for the four functions considering the four previously analyzed normalization radii, ROCI, RMW, R0, R34.

We report all fitted parameters in Table 1 and show the fitted functional forms for f_4 in Figure 5. Regardless of the normalizing radii, the fitted functions show that GHI decays are the strongest closer to the hurricane center and higher hurricane categories. These observations are consistent with the presence of optically thick cloud structures close to the hurricane center and during hurricane maturity and intensification, as noted previously.

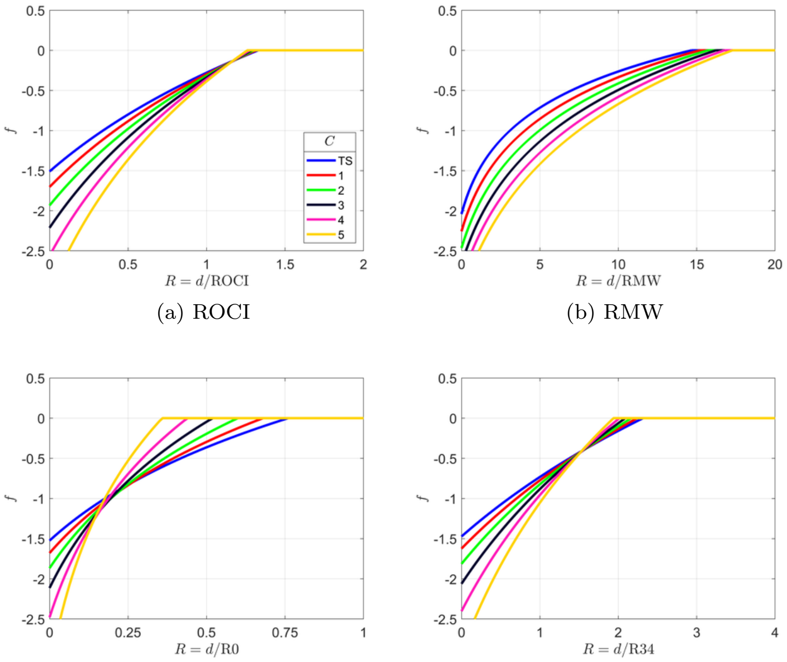

(a) ROCI

(b) RMW

(c) R0

(d) R34

Fig. 5: Fitted functional form f_4 in Equation 5d for distances normalized by the four different normalizing radii.

The regressions also show that the decay extends up to sites well beyond RMW and R34, reaching sites $\sim$ 15RMW and $\sim$ 2ROCI away from the hurricane center. The decay is also well within R0, reaching sites only up to $\sim 0.35 - 0.75$R0. The decay extents are most consistent with ROCI as they are bounded by $\sim$1.3 times its size from the hurricane center (Figure 5a), confirming the observation that the cloud structures and radial extent of hurricane circulation defined by ROCI are strongly coupled with the hurricane mechanism for high light absorption and reflection. Because this threshold ($\sim$ 1.3) does not change significantly for different categories, hurricanes with low categories can cover more extensive regions with clouds that reduce GHI than hurricanes with high categories as long as they have larger ROCI. However, the level of decay will be smaller for lower categories.

3.4 Statistical Performance

We compared the statistical performance of the 16 regressions in Figure 5 using the AIC (Akaike, 1974). The AIC assesses the trade-off between the model goodness of fit and its simplicity. The AIC is estimated as $-2\hat{l} - 2K$,

Table 1: Fitted parameters for the four functional forms of f in Equation 5 using different normalizing radii.

Model	Norm. Radius	Parameters					
		a_1	a_2	b_1	b_2	c_1	c_2
f_1	ROCI	1.38	2.37×10^{-1}	6.43×10^{-1}		1.95	
	RMW	7.78×10^{-1}	8.85×10^{-2}	1.27		1.34×10^{2}	
	R0	6.42×10^{-1}	1.47×10^{-1}	5.45×10^{-2}		1.04	
	R34	1.55	2.45×10^{-1}	1.30		3.43	
f_2	ROCI	1.37	2.46×10^{-1}	6.43×10^{-1}	3.01×10^{-3}	1.95	
	RMW	7.27×10^{-1}	1.08×10^{-1}	9.43×10^{-1}	1.29×10^{-1}	9.74×10^{1}	
	R0	1.63	7.50×10^{-1}	4.66×10^{-1}	4.62×10^{-2}	1.05	
	R34	1.47	3.47×10^{-1}	1.33	5.28×10^{-2}	3.60	
f_3	ROCI	1.34	2.53×10^{-1}	6.47×10^{-1}		2.01	-1.90×10^{-2}
	RMW	8.52×10^{-1}	9.73×10^{-2}	1.69		1.62×10^{1}	5.89×10^{-1}
	R0	7.61×10^{-1}	2.11×10^{-1}	1.06×10^{-1}		9.01×10^{-1}	-8.59×10^{-2}
	R34	1.40	2.90×10^{-1}	1.27		3.64	-7.70×10^{-2}
f_4	ROCI	1.97	9.65×10^{-2}	1.15	-1.26×10^{-1}	2.48	-1.39×10^{-1}
	RMW	7.74×10^{-1}	1.41×10^{-1}	1.02	2.77×10^{-1}	1.57×10^{1}	7.98×10^{-1}
	R0	1.43	8.66×10^{-2}	3.99×10^{-1}	-6.36×10^{-2}	1.16	-1.44×10^{-1}
	R34	2.57	4.96×10^{-2}	2.99	-3.84×10^{-1}	5.31	-4.59×10^{-1}

where $\hat{l}$ is the logarithm of the marginal likelihood and K is the "degrees of freedom correction" equal to the number of fixed parameters plus the number of mean and variance parameters of the random component. K represents a penalty for an increased risk of overfitting with higher model complexity, i.e., with more parameters.

The results show that the model that performs the best (with the lowest AIC score) is f_4 with $R = d/\mathrm{ROCI}$ (Table S2). In fact, for all normalizing radii, f_4, which takes six parameters, performs better than f_3 and f_2, which take 5 parameters, and than f_1, which takes 4 parameters. Moreover, f_3 performs better than f_2 in all cases, suggesting that having a category-dependent scale factor c_2 is more effective than having a category-dependent short-distance correction factor b_2. f_1 performs worse than f_3, but in a few cases, it performs better than f_2.

ROCI and R34, which are the radii with the first and second-best AIC performance (Figure S6), exhibit a similar shape where hurricanes with lower categories take slightly longer distances to reach normal levels of GHI, i.e., $f_4 = 0$. R0, the radius with third-best performance, shows much longer distances to reach the plateau for hurricanes with smaller categories. In contrast, RMW, which has the lowest performance, exhibits smaller extents with GHI decay for hurricanes with lower categories. Based on these AIC scores, we suggest using f_4 with $R = d/\mathrm{ROCI}$ to track GHI decay during hurricanes.

4 Probabilistic modeling of solar irradiance during hurricanes

4.1 Stochastic model formulation

We use stochastic modeling for spatiotemporal simulation of solar irradiance during hurricanes and solve the problem with Monte Carlo simulation. The analysis estimates irradiance during a hurricane h for each site j (out of N sites of interest) and multiple time steps t. Following Equation 3, samples of GHI realizations can be as

$$I^h = \bar{I} \times e^{f(R,C)+\epsilon^h} \tag{8}$$

In the logarithmic space, ϵ^h accounts for spatiotemporal variability in GHI during hurricanes. Under our initial assumption that hurricanes only modify the GHI logarithmic mean, ϵ^h remains the same as normal-conditions ϵ. Thus

$$I^h = \bar{I} \times e^{f(R,C)+\epsilon} \tag{9}$$

Following the lognormality assumption for GHI during normal conditions, I^h can be estimated by transforming GHI during normal conditions to GHI during hurricane conditions

$$I^h = I \times e^{f(R,C)} \tag{10}$$

This equation enables us to leverage well-defined GHI normal-conditions data throughout the entire U.S. to find decayed GHI during hurricanes with a clean and simple formula. We fit probability distributions for I using data from the NREL Physical Solar Model (PSM) version 3 (Sengupta et al., 2018). This 20-year dataset is sufficient to characterize two-hour variations of normal-conditions GHI within a day for each month and up to 4-km spatial resolution. Then, for each site j and time t, a realization of GHI during normal conditions ($\tilde{I}_{t,j}$) is sampled and adjusted to hurricane conditions using $f(R_{t,j}, C_t)$ as

$$\tilde{I}^h_{t,j} = \tilde{I}_{t,j} \times e^{f(R_{t,j},C_t)} \tag{11}$$

4.2 Assessing GHI in the Southern United States for a synthetic storm

We estimated irradiance for 839 counties ($N = 839$) in the United States's southern region for a large hurricane from its genesis to its dissipation, focusing on the counties' centroids. We selected the hurricane from a synthetic dataset with 5018 physically possible landfalling storms in the U.S. generated from a statistical-deterministic tropical cyclone (TC) model (Marsooli et al., 2019). The selected synthetic storm reaches a category of 5 before making landfall in Florida affecting a large region, e.g., ROCI of ∼500 km (Figure 6a).

The model output the hurricane's track, maximum sustained winds, and radii of maximum winds in 2-hour intervals, which were coupled with irradiance estimates using the exact synthetic hurricane's temporal resolution. Additionally, at each time step, we estimated R0 based on both the radius of maximum wind and maximum wind using the same TC wind field profile model applied to the historical storms (Chavas et al., 2015). We estimated ROCI using the expression ROCI = 0.18 × R0 + 226 (km), which was obtained conducting a regression on the 22 historic TC described previously. This application illustrates how our proposed framework combines synthetic storm simulations, irradiance quantification, and our proposed GHI decay model.

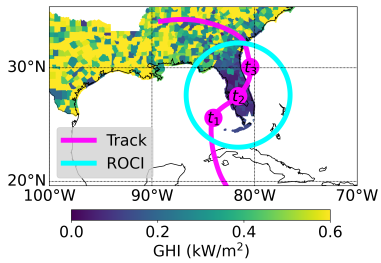

(a) Spatial simulation

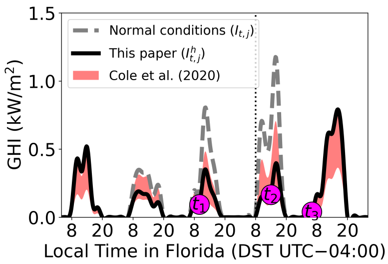

(b) Temporal simulation

Fig. 6: Stochastic simulation of GHI during a synthetic storm making landfall in Florida. The spatial simulation shows a GHI map at 2 pm local time (DST UTC -4), i.e., t_2, when the hurricane has a category of 4 and a ROCI of ∼500 km. The temporal simulation shows GHI during the storm in black for the Miami-Dade county (white star in the map). The circle marks in magenta show the GHI in Miami-Dade for the times when the hurricane center was at corresponding circle marks for times t_1, t_2 , and t_3 in the map. The hurricane takes 44 hours to go from t_1 to t_2. A vertical dotted line depicts landfall time.

A snapshot map shows the resulting GHI, $\tilde{I}^h_{t,j}$, for 2 pm local time, i.e., fixed t, when the storm crossing Florida from West to East (Figure 6a). Under normal conditions, GHI would be high at 2 pm, similar to the levels of Texas or Louisiana on the map, with several regions above 0.6 kW/m^2. However, our simulations show that the hurricane significantly reduces generation to values even below 0.1 kW/m^2 close to the hurricane center. Note that cloud conditions of category-4 hurricanes drastically reduce the median GHI by 70%, i.e., $f_4 = -1.21$, even at distant sites 0.5ROCI away from the hurricane center (Figure 5a). The resulting spatial distribution shows a good resemblance with the radial decay during the 2005 Hurricane Katrina with significantly lower GHI in the areas surrounding the hurricane center (Figure 1a).

The simulation of multiple snapshots allows for the analysis of the temporal variations of GHI during hurricanes at a specific site, i.e., fixed j. In Miami-Dade county (in the white star in Figure 6b), Florida, the hurricane decreased GHI before making landfall. The simulation shows that the hurricane reduces GHI, $\tilde{I}^h_{t,j}$, during three days. Through an analysis of 18 previous hurricanes, Cole et al. (2020) noted that GHI decayed to 18-60%, from clear-sky GHI during storms, and 39%-90% and 46%-100% for 72 hours before and after storms. The event duration in that study was determined through a subjective assessment of extreme wind conditions, resulting in an estimated average duration of 44 hours for the 18 events.

For comparison, we estimated the range of GHI decay using Cole et al. (2020)'s ratios, assuming that the synthetic storm's critical effects on Miami-Dade also last 44 hours. Our results give GHI estimates within Cole et al. (2020)'s ranges, indicating consistency with these observations, for the three days when our model predicts hurricane affects irradiance in Miami-Dade. Nevertheless, Cole et al. (2020)'s study suggests that the hurricane will affect GHI for five days, two more days than our model. These differences are not significant in the final estimates of GHI, though, as Cole et al. (2020) observed that GHI reductions before and after storms can also be modest, 10% and below. These slight differences arise from the subjective definition of the hurricane duration in Cole et al. (2020)'s study. Defining a high threshold for extreme hurricane winds would reduce the hurricane duration, further reducing the timespan of decayed GHI.

Finally, our model demonstrates how irradiance can be simulated under hurricane conditions using state-of-the-art hurricane hazard characterizations. Our study systematically assesses instantaneous hurricane conditions through intensity and radii. Thus, it allows us to model higher temporal resolution than Cole et al. (2020)'s three intervals by coupling synthetic storms and irradiance quantification methods to assess solar irradiance during these extreme events. While the application focuses on a single synthetic storm, our framework allows for the assessment of the entire hurricane dataset to analyze comprehensive risk metrics (Ceferino et al., 2021).

5 Conclusions

This paper presents a stochastic model to capture irradiance decay during hurricanes, which has not been developed before to the authors' knowledge. The irradiance decay model is based on an extensive assessment of GHI under 22 landfalling storms in the North American basin, which reached a category of at least three during their lifetime. The dataset conclusively shows that hurricanes reduce GHI throughout their tracks. We confirmed that the distance from a site to the hurricane and its category are critical predictors of irradiance decay. We argue that the mechanism driving the decay is the formation of optically thick clouds in the eyewall, which often become thicker during hurricane intensification. With high moisture density and vertical depth, these optically thick clouds reduce direct incident radiation by light absorption and reflection.

We fitted four functional forms that vary in complexity to represent irradiance decay using a mixed-effects regression. Multiple category-dependent features controlling the intensity and shape of decay were tested, and the best functional form was selected using AIC to demonstrate its suitable statistical performance. ROCI is shown to be a good size metric for normalizing the distance in the functional forms of irradiance decay. Thus, we suggest using ROCI if hazard modeling allows for its estimation in synthetic future storms.

Next, we described the application of the GHI decay model for stochastic simulations of solar irradiance during hurricanes. We conducted a spatiotemporal simulation of GHI during a synthetic storm for the United States's southern region in 839 counties. Our analysis shows to be consistent with empirical observations of GHI spatial and temporal distributions from previous datasets and studies. Our results show that solar irradiance can decrease by more than 70% in vast regions during a category-4 hurricane. Furthermore, reductions in irradiance lasted three days for Miami-Dade in our analysis, suggesting that power loss can last several days. These results indicate that hurricanes can significantly affect generation even if the solar infrastructure is undamaged. Damage to the solar infrastructure will further exacerbate the losses reducing generation to zero even if irradiance bounces back to normal after the hurricane. Thus, comprehensive generation loss assessments require the integration with and development of panel fragility functions as in Ceferino et al. (2021)'s study.

Our results show that generation losses driven by GHI decay can be critical, e.g., 70%. Functional power systems are crucial to support other urban systems during emergency response and expedite recovery. Recently, Hurricane Ida caused nearly 1M outages in Louisiana, reducing electricity access by more than 60% in more than ten parishes (counties), affecting the functionality of the water system and delaying recovery Goodman et al. (2021); Prevatt et al. (2021). While our proposed model focuses on spatiotemporal forecasting of irradiance rather than solar generation, it is essential to assess the effect of power disruptions during hurricanes due to the importance of irradiance decay. Solar generation is expected to become an essential source for our future power systems. At the same time, hurricanes are projected to be stronger in the future climate (Knutson et al., 2020). Coupling the presented model with risk frameworks offers opportunities to assess the effectiveness of climate mitigation and adaptation measures to make our grid more resilient to natural hazards while it becomes cleaner with solar energy.

Declarations

Funding

We acknowledge the financial support by the Andlinger Center for Energy and the Environment at Princeton University through the Distinguished Postdoctoral Fellowship. Additionally, this research was also supported by the NSF Grants 1520683 and 1652448. The authors are grateful for their generous support.

Conflict of interest

The authors declare that they have no conflict of interest.

Availability of data and material

The GHI data are publicly available and were obtained from the NREL website (`https://www.nrel.gov/gis/solar.html`) using the corresponding API. The historical hurricane data are publicly available and were obtained from the National Hurricane Center website (`https://www.nhc.noaa.gov/data/`) The parameters for the fitted GHI decay model, Figures S1-S6 and Tables S1 and S2 are provided in the Supplementary Information in `https://tinyurl.com/4nsbz8dc`.

Code availability

The code with the model implementation from this paper is available upon request to the corresponding author.

Author contributions

L.C. and N.L. conceptualized the model for GHI decay and the application for assessing solar irradiance during hurricanes. L.C., N.L., and D.X. curated the data for irradiance during storms, processed wind fields, and fitted the statistical models for the GHI decay model. L.C. drafted the manuscript with contributions and edits from all the authors.

References

Abrahamson N, Gregor N, Addo K (2016) BC hydro ground motion prediction equations for subduction earthquakes. Earthquake Spectra 32(1):23–44, DOI 10.1193/051712EQS188MR

Akaike H (1974) A new look at the statistical model identification. IEEE Transactions on Automatic Control 19(6):716–723, URL https://ieeexplore.ieee.org/stamp/stamp.jsp?tp={&}arnumber=1100705

Campbell KW, Bozorgnia Y (2014) NGA-West2 ground motion model for the average horizontal components of PGA, PGV, and 5% damped linear acceleration response spectra. Earthquake Spectra 30(3):1087–1114, DOI 10.1193/062913EQS175M

Campbell RJ, Clark CE, Andrew Austin D (2018) Repair or Rebuild: Options for electric power in Puerto Rico. Tech. rep., Congressional Research Service

Ceferino L, Liu C, Alisjahbana I, Patel S, Sun T, Kiremidjian A, Rajagopal R (2020) Earthquake resilience of distributed energy resources. In: 17th World Conference on Earthquake Engineering, Tokyo, Japan

Ceferino L, Lin N, Xi D (2021) Bayesian Updating of Solar Panel Fragility Curves and Implications of Higher Panel Strength for Solar Generation Resilience

Chavas DR, Lin N, Emanuel K (2015) A model for the complete radial structure of the tropical cyclone wind field. Part I: Comparison with observed structure. Journal of the Atmospheric Sciences 72(9):3647–3662, DOI 10.1175/JAS-D-15-0014.1

Cole W, Greer D, Lamb K (2020) The potential for using local PV to meet critical loads during hurricanes. Solar Energy 205(May):37–43, DOI 10.1016/j.solener.2020.04.094, URL https://doi.org/10.1016/j.solener.2020.04.094

Colson CM, Nehrir MH, Gunderson RW (2011) Distributed multi-agent microgrids: A decentralized approach to resilient power system self-healing. Proceedings - ISRCS 2011: 4th International Symposium on Resilient Control Systems pp 83–88, DOI 10.1109/ISRCS.2011.6016094

Creutzig F, Agoston P, Goldschmidt JC, Luderer G, Nemet G, Pietzcker RC (2017) The underestimated potential of solar energy to mitigate climate change. Nature Energy 2(9), DOI 10.1038/nenergy.2017.140, 1710.05957

Devabhaktuni V, Alam M, Shekara Sreenadh Reddy Depuru S, Green RC, Nims D, Near C (2013) Solar energy: Trends and enabling technologies. Renewable and Sustainable Energy Reviews 19:555–564, DOI 10.1016/j.rser.2012.11.024, URL http://dx.doi.org/10.1016/j.rser.2012.11.024

Goodman JD, Heyward G, Kasakove S (2021) Louisiana's governor tells evacuees not to return until infrastructure is restored. URL https://www.nytimes.com/live/2021/08/31/us/hurricane-ida-updates

Henry D, Ramirez-Marquez JE (2016) On the Impacts of Power Outages during Hurricane Sandy—A Resilience-Based Analysis. Systems Engineering 19(1):59–75, DOI 10.1002/sys.21338, URL https://onlinelibrary.wiley.com/doi/10.1002/sys.21338

Houze RA (2010) Clouds in tropical cyclones. Monthly Weather Review 138(2):293–344, DOI 10.1175/2009MWR2989.1

International Energy Agency (2014) Energy Technology Perspectives 2014 (Harnessing Electricity's Potential) p 382, DOI 10.1787/energy_tech-2010-en

John J, Shukla BP, Gajjar PN, Sathiyamoorthy V (2020) Study of satellite-derived cloud microphysical parameters for tropical cyclones over the North Indian Ocean (2010–2013). Theoretical and Applied Climatology 139(3-4):1163–1173, DOI 10.1007/s00704-019-03047-9

Kannan N, Vakeesan D (2016) Solar energy for future world: - A review. Renewable and Sustainable Energy Reviews 62:1092–1105, DOI 10.1016/j.rser.2016.05.022

Knutson T, Camargo SJ, Chan JC, Emanuel K, Ho CH, Kossin J, Mohapatra M, Satoh M, Sugi M, Walsh K, Wu L (2020) Tropical cyclones and climate change assessment part II: Projected response to anthropogenic warming. Bulletin of the American Meteorological Society 101(3):E303–E322, DOI 10.1175/BAMS-D-18-0194.1

Kokhanovsky AA, von Hoyningen-Huene W (2004) Optical properties of a hurricane. Atmospheric Research 69(3-4):165–183, DOI 10.1016/j.atmosres.2003.09.005

Landsea CW, Franklin JL (2013) Atlantic hurricane database uncertainty and presentation of a new database format. Monthly Weather Review 141(10):3576–3592, DOI 10.1175/MWR-D-12-00254.1

Lehr J, Vrettos E, Rajagopal R, Jain R, Everts M (2017) Financial Viability of Residential Photovoltaic and Battery Systems in Californias. Journal of Management and Sustainability 7(4):16, DOI 10.5539/jms.v7n4p16, URL `http://www.ccsenet.org/journal/index.php/jms/article/view/71394`

Lindstrom MJ, Bates DM (1990) Mixed Effects Models for Repeated Measures Data. Biometrics 46(3):673–687, DOI 10.1111/j.1541-0420.2005.00440.x

Liou KN (2002) An Introduction to Atmospheric Radiation. Elsevier

Luo Z, Stephens GL, Emanuel KA, Vane DG, Tourville ND, Haynes JM (2008) On the use of CloudSat and MODIS data for estimating hurricane intensity. IEEE Geoscience and Remote Sensing Letters 5(1):13–16, DOI 10.1109/LGRS.2007.905341

Marsooli R, Lin N, Emanuel K, Feng K (2019) Climate change exacerbates hurricane flood hazards along US Atlantic and Gulf Coasts in spatially varying patterns. Nature Communications 10(1):1–9, DOI 10.1038/s41467-019-11755-z, URL `http://dx.doi.org/10.1038/s41467-019-11755-z`

Mihailović DT, Aksentijevic A, Mihailović A (2021) Mapping regularities in the solar irradiance data using complementary complexity measures. Stochastic Environmental Research and Risk Assessment 35(6):1257–1272, DOI 10.1007/s00477-020-01955-1

Moriarty P, Honnery D (2016) Can renewable energy power the future? Energy Policy 93:3–7, DOI 10.1016/j.enpol.2016.02.051, URL `http://dx.doi.org/10.1016/j.enpol.2016.02.051`

Nouri B, Wilbert S, Segura L, Kuhn P, Hanrieder N, Kazantzidis A, Schmidt T, Zarzalejo L, Blanc P, Pitz-paal R (2019) Determination of cloud transmittance for all sky imager based solar nowcasting Transmittance known Transmittance unknown. Solar Energy 181(February):251–263, DOI 10.1016/

j.solener.2019.02.004, URL https://doi.org/10.1016/j.solener.2019.02.004

Panteli M, Mancarella P (2015) The grid: Stronger, bigger, smarter?: Presenting a conceptual framework of power system resilience. IEEE Power and Energy Magazine 13(3):58–66, DOI 10.1109/MPE.2015.2397334

Patel S, Rasouli M, Qin J, Rajagopal R, Science C (2018) The Value of Distributed Energy Resources for Heterogeneous Residential Consumers pp 1–24, URL https://arxiv.org/abs/1709.08140, arXiv:1709.08140v4

Patel S, Ceferino L, Liu C, Kiremidjian A, Rajagopal R (2021) The disaster resilience value of shared rooftop solar systems in residential communities. Earthquake Spectra p 875529302110200, DOI 10.1177/87552930211020020

Perea A, Smith C, Davis M, Mond A, Gallagher B, Rumery S, Holm A, Goldstein R, Baca J (2019) U. S. Solar Market Insight Executive Summary. Tech. rep., Wood Mackenzie & Solar Energy Industries Association —, Mackenzie2020

Pinheiro J, Bates D (2006) Mixed-Effect Models in S and S-PLUS. Springer Science & Business Media

Prevatt D, Kameshwar S, Roueche D, Rittelmeyer B, Duarte T, Heo T, Ibrahim H, Klepac S, Lafontaine O, Lin T, Manuel L, Pilkington S, Pinyochotiwong Y, Santiago-Hernandez J, Strader S, Gurley K, Kijewski-Correa T, Mosalam K, Robertson I (2021) StEER: Hurricane Ida Joint Preliminary Virtual Reconnaissance Report - Early Access Reconnaissance Report (PVRR-EARR). Tech. Rep. August, DOI 10.17603/ds2-w6km-fe51

Sengupta M, Xie Y, Lopez A, Habte A, Maclaurin G, Shelby J (2018) The National Solar Radiation Data Base (NSRDB). Renewable and Sustainable Energy Reviews 89(March 2018):51–60, DOI 10.1016/j.rser.2018.03.003, URL https://doi.org/10.1016/j.rser.2018.03.003

Shah V, Booream-Phelps JC (2015) Crossing the Chasm: Solar Grid Parity in a Low Oil Price Era. Tech. rep., Deutsche Bank, URL https://www.db.com/cr/en/concrete-deutsche-bank-report-solar-grid-parity-in-a-low-oil-price-era.htm

Solangi KH, Islam MR, Saidur R, Rahim NA, Fayaz H (2011) A review on global solar energy policy. Renewable and Sustainable Energy Reviews 15(4):2149–2163, DOI 10.1016/j.rser.2011.01.007, URL http://dx.doi.org/10.1016/j.rser.2011.01.007

Solaun K, Cerdá E (2019) Climate change impacts on renewable energy generation. A review of quantitative projections. Renewable and Sustainable Energy Reviews 116(109415), DOI 10.1016/j.rser.2019.109415

The International Renewable Energy Agency (2018) Global Energy Transformation: A Rodmap to 2050. Tech. rep., The International Renewable Energy Agency

Wang Y, Chen C, Wang J, Baldick R (2016) Research on Resilience of Power Systems under Natural Disasters - A Review. IEEE Transactions on Power Systems 31(2):1604–1613, DOI 10.1109/TPWRS.2015.2429656

Wang Z, Román MO, Sun Q, Molthan AL, Schultz LA, Kalb VL (2018) Monitoring Disaster-Related Power Outages Using Nasa Black Marble Nighttime Light Product. ISPRS - International Archives of the Photogrammetry, Remote Sensing and Spatial Information Sciences XLII-3:1853–1856, DOI 10.5194/isprs-archives-XLII-3-1853-2018, URL https://doi.org/10.5194/isprs-archives-XLII-3-1853-2018%0Ahttps://www.int-arch-photogramm-remote-sens-spatial-inf-sci.net/XLII-3/1853/2018/

Weatherford C, Gray W (1988) Typhoon Structure as Revealed by Aircraft Reconnaissance. Part II: Structural Variability. Monthly Weather Review 116(5):1044–1056., DOI 10.16309/j.cnki.issn.1007-1776.2003.03.004

Xie Y, Sengupta M, Dudhia J (2016) A Fast All-sky Radiation Model for Solar applications (FARMS): Algorithm and performance evaluation. Solar Energy 135:435–445, DOI 10.1016/j.solener.2016.06.003, URL http://dx.doi.org/10.1016/j.solener.2016.06.003

Xie Y, Sengupta M, Wang C (2019) A Fast All-sky Radiation Model for Solar applications with Narrowband Irradiances on Tilted surfaces (FARMS-NIT): Part II. The cloudy-sky model. Solar Energy 188(June):799–812, DOI 10.1016/j.solener.2019.06.058, URL https://doi.org/10.1016/j.solener.2019.06.058